Acoustic signals in air and water generated by very shallow marine seismic sources: An experimental study

Daniel Wehner, U. Peter Svensson, and Martin Landrø

Citation: The Journal of the Acoustical Society of America **147**, 1092 (2020); doi: 10.1121/10.0000691
View online: https://doi.org/10.1121/10.0000691
View Table of Contents: https://asa.scitation.org/toc/jas/147/2
Published by the Acoustical Society of America

JASA ARTICLE

Acoustic signals in air and water generated by very shallow marine seismic sources: An experimental study

Daniel Wehner,[1,a)] U. Peter Svensson,[2] and Martin Landrø[2]
[1]*Department of Geoscience and Petroleum, NTNU, Trondheim, 7031, Norway*
[2]*Department of Electronic Systems, NTNU, Trondheim, 7491, Norway*

ABSTRACT:
When a marine seismic source, like an airgun, is fired close to the water surface the oscillating bubble interacts with the water–air interface. The main interest for seismic applications is how this effect impacts the acoustic signal propagating into the water. It is known that the sound transmission into air is abnormally strong when the sound source is very close to the sea surface relative to the emitted wavelength. Detailed insight into how the acoustic signal changes when the source depth is changed is useful in seismic data analysis and processing. Two experiments are conducted in a water tank with two different types of seismic sources. In experiment A the source is a small cavity that is sufficiently far away from the water–air interface so that it can be assumed that no interaction between the cavity and water surface occurs. In experiment B the source is a larger air bubble that is very close to the water–air interface, and hence interaction between the bubble and water surface occurs. The effects on the water surface, oscillating bubble, and emitted acoustic pressure into air are discussed. It is demonstrated that the moving surface contributes significantly to the acoustic signal measured in air. © *2020 Acoustical Society of America*.
https://doi.org/10.1121/10.0000691
(Received 25 September 2019; revised 9 January 2020; accepted 21 January 2020; published online 13 February 2020)
[Editor: Nicholas P. Chotiros] Pages: 1092–1103

I. INTRODUCTION

In marine seismic acquisition and underwater acoustics the focus is naturally on the sound pressure wave that propagates in water. However, a part of the sound pressure wave is also transmitted into the air. The fraction of the signal that is transmitted depends, among other things, on the distance between the source and the water–air interface. For an oscillating bubble as the source, the bubble interacts and disturbs the water surface when excited close to the interface and the moving interface could emit additional sound waves into the air. Hence, we might define two main effects that radiate sound waves into the air. First, a sound pressure wave is transmitted through the interface. Second, the water surface is set into motion by the expanding bubble and radiates a sound wave into the air. How strong the signals are that are transmitted into the air, and reflected back into the water, respectively, is of interest in marine seismic applications. Here, the sources are close to the water–air interface and the signal that is reflected back into the water has a major impact on the measured data (Amundsen *et al.*, 2017; Landrø and Amundsen, 2014; Wehner *et al.*, 2019).

The signal that is transmitted through an interface depends on the transmission coefficient of the interface. For the water–air interface the transmission coefficient is low due to the high impedance contrast between water and air (Kinsler *et al.*, 1962). For plane waves incident on the interface the transmission depends on the angle of incidence, while for spherical waves incident on the interface it depends also on the frequency, source-interface, and interface-receiver distance (Aki and Richards, 2002; Brekhovskikh and Lysanov, 1991). The strongest difference between a spherical transmission response and the plane wave transmission coefficient could be observed for low frequencies, or more precisely for wavelengths larger than the source-interface distance as demonstrated by Li *et al.* (2017a, 2017b) and Yan *et al.* (2017) for amplitude versus offset analysis of seismic data between two acoustic media. In addition, an increased amount of the acoustic signal could be transmitted into air caused by the evanescent component of the wave inside water which can be converted to a homogeneous wave in air for particular wave numbers. This is discussed in theory for monopole sound sources in water where the source depth is much less than the emitted acoustic wavelength by Godin (2006), McDonald and Calvo (2007), Godin (2008), and Glushkov *et al.* (2013). Experimental results verifying the increased transmission from water into air, when accounting for evanescent waves, for a frequency range between 1 and 20 kHz are presented by Calvo *et al.* (2013), Voloshchenko and Tarasov (2013), and Voloshchenko and Tarasov (2019). We like to mention that reversed experiments for the transmission from air to water are presented by several authors. The transmission from a sonic boom generated by an aircraft at different elevations above the ocean is investigated by Sohn *et al.* (2000). Lubard and Hurdle (1976) demonstrate the increased transmission from a speaker source in air caused by a rougher ocean surface.

[a)]Electronic mail: daniel.wehner@t-online.de, ORCID: 0000-0001-8459-6179.

https://doi.org/10.1121/10.0000691

The behaviour of oscillating bubbles and explosions close to the water–air interface is studied by several authors for different sizes of air bubbles and an overview of bubble dynamics and potential applications is given by Wang *et al.* (2018). The interaction of the free surface with small bubbles, in the millimeter range up to a few centimeters, is demonstrated by Oguz and Prosperetti (1990), Chahine *et al.* (1995), and Krieger and Chahine (2005). A critical distance where the interaction between the bubble and free surface takes place is theoretically and experimentally investigated by Chahine (1977). The effect of surface tension on the water–air interface displacement caused by the bubble and acoustic pressure is demonstrated by Lu *et al.* (1989) and Cinbis *et al.* (1993). When small bubbles burst at the water–air interface a jet is formed as presented by Boulton-Stone and Blake (1993) in a numerical model and experimentally demonstrated by Blake and Gibson (1981) and Longuet-Higgins (1983). The interaction between the free surface and intermediate bubble radii, in the range of a few tens of centimeters, is demonstrated by Hung and Hwangfu (2010) and Cui *et al.* (2016) using small explosives. They also investigate the interaction with solid boundaries. High-speed photography for these experiments indicates cavitation near the surface due to the negative acoustic pressure reflected from the surface and the formation of a jet through the bubble (Cui *et al.*, 2016). Experiments with a small laboratory scale airgun fired close to a solid boundary and free surface are conducted by de Graaf *et al.* (2014). The interaction between the ocean surface and large spherical underwater blasts emitting a shock wave is theoretically described by Chan *et al.* (1968), Collins and Holt (1968), and Ballhaus and Holt (1974). Another example of the interaction between a fluid-air interface and large bubbles, in the range of a few meters, is related to volcanic eruptions. The infrasound signal recorded from gas bubbles breaking at the surface of a lava column is presented by Vergniolle and Brandeis (1994, 1996), Vergniolle *et al.* (1996), and Johnson (2003).

Here, we compare the results of two experiments with different marine seismic sources and the focus is on the acoustic signal that is recorded in air. The main difference between the experiments is the bubble size created by the source. In experiment A the radius of the cavity generated by a watergun is small, approximately 2–3 cm, and the distance between the cavity and water–air interface is large relative to the cavity radius. Therefore, no interaction between the source and the water surface is expected for the source depths in the experiment. In experiment B the radius of the bubble generated by an airgun is much larger, approximately 20–25 cm, and hence the bubble strongly interacts with the water surface when excited at depths smaller than 4 times the maximum bubble radius. Three different scenarios of source-interface interaction can be defined: (1) only the acoustic pressure is transmitted through and reflected from the interface and superpose with the down-going acoustic signal from the oscillating bubble, (2) the water–air interface is set into motion by the oscillating bubble, and (3) the air bubble bursts at the water surface into the air. We investigate how the interaction between the source and the water–air interface influences the acoustic signal emitted into air and focus on scenarios (2) and (3).

II. THEORY

The two main effects, signal transmission through the water–air interface and an acoustic signal emitted by a moving surface, are briefly discussed in the following.

The acoustic pressure from a source underwater transmitted through the water–air interface and measured in air can be described for a flat fluid-fluid interface and plane waves as (Kinsler *et al.*, 1962)

$$p_t = p_i T_c \exp[i(\omega t - k_a x \sin(\theta_a) - k_a z \cos(\theta_a))], \quad (1)$$

where p_i is the pressure incident on the water–air interface, T_c is the transmission coefficient, θ_a is the angle of refraction in air, and $k_a = \omega/c_a$ where c_a is the sound velocity in air and $\omega = 2\pi f$ with f as the frequency. The coordinates x and z are as shown in Fig. 1.

The acoustic pressure in air generated from a moving surface could be computed similar to a vibrating membrane as (Harris, 1981)

$$p_m(t) = \frac{\rho_a}{2\pi}\int_{dS} \frac{\ddot{h}\left(t - \frac{r_a}{c_a}\right)}{r_a} dS, \quad (2)$$

where ρ_a is the density of air, dS is a surface element in the horizontal plane of the water surface, r_a is the distance from the water surface to the receiver, and $\ddot{h}$ is the second time derivative of the water surface displacement h (Fig. 1). The surface displacement caused by an oscillating bubble is related to the distance of the source from the water surface and the bubble size (Chahine, 1977). Here, we use an *ad hoc* model for the surface displacement accounting for these components, similar to the model presented by Chahine (1977) and adjusted to the experimental observations, as

$$h = \frac{R_m}{5(r^2 + z_s^2)^{3/2}} \frac{4}{3}\pi R^3, \quad (3)$$

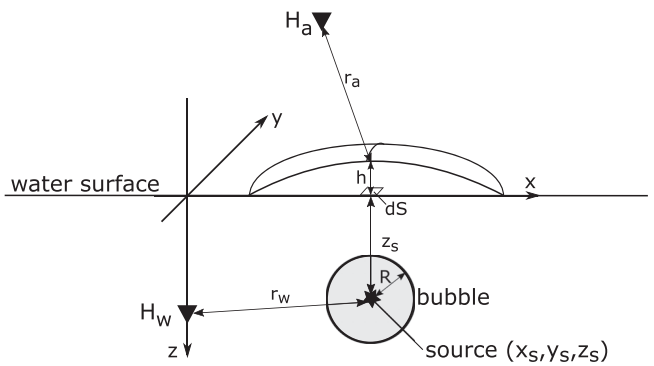

FIG. 1. Sketch illustrating the displacement h of the water surface caused by an oscillating bubble underwater. The receiver in air and water are denoted as H_a and H_w, respectively.

where $r = \sqrt{(x - x_s)^2 + (y - y_s)^2 + z_s^2}$ is the distance between the center of the bubble and the horizontal plane at the water–air interface, R is the bubble radius, and R_m is the maximum bubble radius (Fig. 1). It should be noted that the model presented by Chahine (1977) is derived for small cavities and it is valid under the assumption that the bubble is sufficiently far from the water–air interface, so that it can be represented as an oscillating source of variable intensity with time. As this requirement is not always fulfilled for our experiments we note that Eq. (3) is used as a phenomenological model adjusted to our experiments. The water surface displacement caused by an oscillating air bubble underwater is illustrated in Fig. 1.

III. EXPERIMENTS

The experiments are conducted in a water tank with the dimensions given in Figs. 2 and 3. The walls of the tank are equipped with 5 cm thick foam mattresses. The mattresses do not act as perfectly absorbing boundaries, but reduce the impact of wall reflections. However, the main peak of the source signal from an air gun does not vary significantly between experiments performed in the tank and free field as demonstrated by Langhammer and Landrø (1996). The Brüel & Kjær hydrophones of type 8105 (Nærum, Denmark), which are used as receivers for all experiments in the tank, have a flat frequency response from 0.1 Hz to 100 kHz. Additional hydrophones of the same type are located in air to record the signal transmitted through the water–air interface. The hydrophones of type 8105 have the same sensitivity in water and air for frequencies up to 3 kHz. Two different experiments are conducted that mainly differ in the seismic source used for the experiment.

In experiment A, an S15 watergun from Sercel (Nantes, France) with one cylindrical gun port and a gun volume of 15 in^3 (ca. 0.25 l) is used (Fig. 2). The source creates a collapsing cavity caused by a high velocity water jet that is pushed out of the gun port when fired. The maximum radius of the cavity in our experiment is in the range of approximately 2–3 cm (Fig. 2). The source is fired at different depths ranging from $z_s = 0.2$ m to $z_s = 0.7$ m. Therefore, we expect that only the acoustic pressure interacts with the water–air interface (scenario 1).

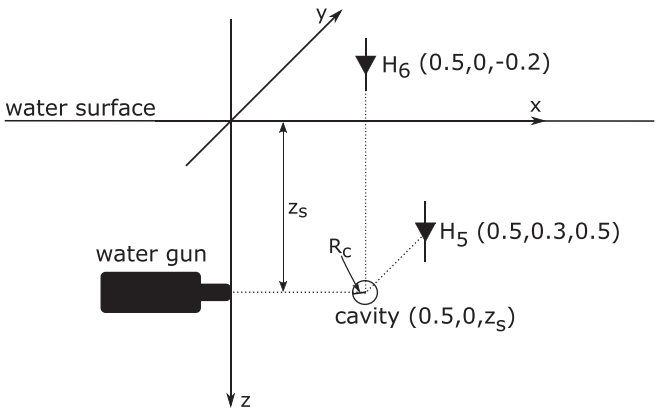

FIG. 2. Sketch of experimental setup in the water tank for experiment A. The hydrophones are indicated as H_5 and H_6 where the x-, y-, and z-coordinates in meters are given in brackets. The water depth in the tank is 1.25 m and the width (y-direction) and length (x-direction) of the tank are 2.5 and 6 m, respectively.

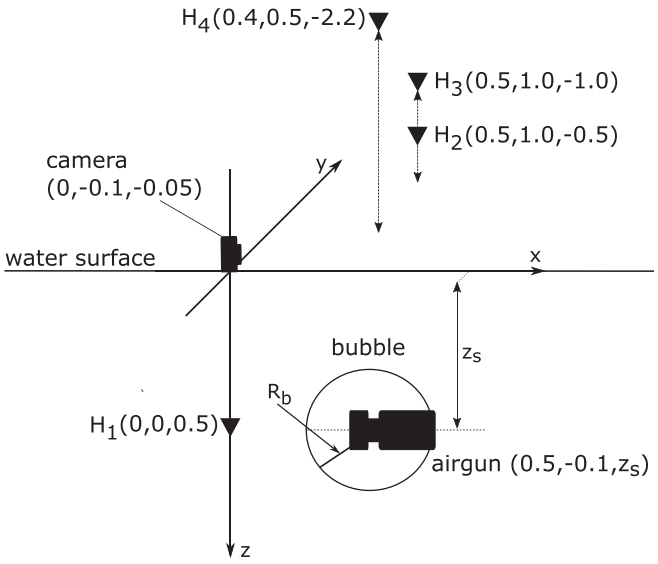

FIG. 3. Sketch of experimental setup in the water tank for experiment B. The hydrophones are indicated as H_1, H_2, H_3, and H_4 where the x-, y-, and z-coordinates in meters are given in brackets. The water depth in the tank is 1.25 m and the width (y-direction) and length (x-direction) of the tank are 2.5 and 6 m, respectively.

In experiment B, a Mini G. Gun from Sercel (Nantes, France) with four gun ports and a chamber volume of 12 in^3 (0.2 l) is used (Fig. 3). The source creates an oscillating air bubble caused by the sudden release of highly compressed air from the gun chamber. The maximum radius of the bubble in our experiment is in the range of approximately 20–25 cm (Fig. 3). The source is fired at different depths ranging from $z_s = 0.1$ m to $z_s = 0.6$ m. In addition to the pressure recordings, a camera is placed slightly above the water–air interface during this experiment to film the water surface while the airgun is fired at different depths. The recording rate of the camera is 240 frames per second which allows having a photo approximately every 4.2 ms. For this experiment we expect a strong physical interaction between the oscillating bubble and the water–air interface (scenarios 2 and 3).

IV. RESULTS

A. Measurements

First, we compare the recordings in air from both experiments. Second, we investigate the results from experiment B in more detail as the source strongly interacts with the water–air interface which is not the case for experiment A. The pressure recordings in water and air are shown in Figs. 4 and 5 for experiment A and B, respectively. The maximum bubble radius indicated in the figures for the cavity R_{mc} and airgun bubble R_{mb} is estimated from the measured collapse time τ (Rayleigh, 1917)

$$\tau = 0.915 R_m \sqrt{\frac{\rho_w}{p_0}}, \tag{4}$$

https://doi.org/10.1121/10.0000691

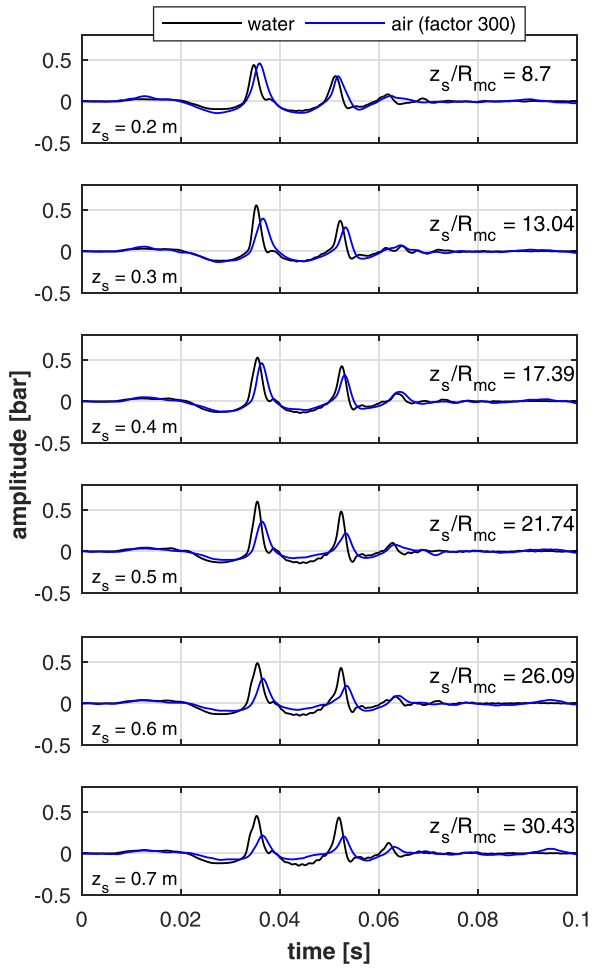

FIG. 4. (Color online) Measurements of watergun signature at H_5 and H_6 (Fig. 2) for different source depths z_s in experiment A. Indicated is also the ratio between the source depth z_s and maximum cavity radius R_{mc}. Signal is 300 Hz low-pass filtered. The watergun is triggered at $t = 0$ s.

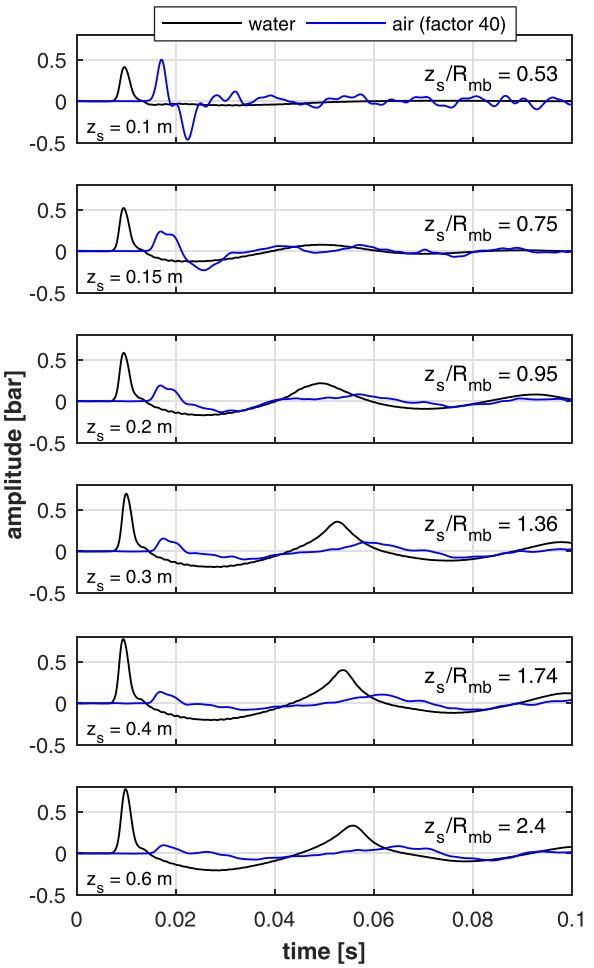

FIG. 5. (Color online) Measurements of airgun signature at H_1 and H_4 (Fig. 3) for different source depths z_s in experiment B. Indicated is also the ratio between the source depth z_s and maximum bubble radius R_{mb}. Signal is 300 Hz low-pass filtered. The airgun is triggered at $t = 0.007$ s.

where ρ_w is the water density, p_0 is the hydrostatic pressure, and 0.915 is an exact number derived from gamma functions by Rayleigh (1917). The radius R_m is replaced by R_{mc} or R_{mb} for the respective experiment. It should be noted that the signals are corrected for geometrical spreading with $1/r$ and that the signal in air is enhanced by multiplication with a constant factor to make it comparable with the recordings in water.

For experiment A the acoustic signal in air is multiplied by 300 (Fig. 4). The signal measured in air has nearly the same shape as the signal in water. The delay between the signals fits with the delay corresponding to the difference in source-receiver distances and different sound velocities in water and air. As the similarity between the acoustic signal in air and water is high, the signal in air is most likely caused by transmission through the interface only (scenario 1). That sound transmission from water to air is the only mechanism is also in agreement with the distance between the source and water–air interface, where the shallowest source is still at a depth larger than 8 times the maximum cavity radius R_{mc}. Therefore, no interaction between the interface and cavity is expected (Chahine, 1977) and it is not observed in the experiments. The acoustic signal reflected from the water–air interface does not alter the shape of the recordings in water too much as demonstrated in a modeled scenario (Wehner *et al.*, 2018). They compare the computed acoustic signal including an air–water interface with the signal in a homogeneous water medium.

For experiment B the acoustic signal in air is multiplied by 40 (Fig. 5) which indicates that the signal in air is stronger than in experiment A relative to the signal strength in water. For the range with comparable source depths z_s in both experiments between 0.2 and 0.6 m, the signal in air in experiment B is about 2 to 2.5 times stronger than in experiment A relative to the signal in water. For shallower source depths the increase of the acoustic signal in air is much stronger and for the shallowest depths of 0.1 m the amplitude in air is doubled compared to the second shallowest depth of 0.15 m (Fig. 5). In addition, we observe that the signal shape is quite different between the measurements in air and water, especially for the shallowest source depths. That is related to the breaking of the air gun bubble into the surrounding air at the water surface (scenario 3). We note a strong negative peak around 0.023 and 0.026 s in air for

source depths of 0.1 and 0.15 m which is not visible in the measurements in water. The measured time delay between the positive main peak in water and air for all source depths is between 7.2 and 7.5 ms which are slightly more than 6.5–6.8 ms which is expected from the source-receiver distance and sound velocity in air. If we account for an error in the acquisition geometry of ± 0.1 m for the position of the receivers the expected time delay can vary by 0.6 ms. As this is within our accuracy achieved in the experiments the measured time delay still fits to the transmitted acoustic signal through the water–air interface. In addition, the main peak in air around 0.018 s is also broadened for source depths between 0.15 and 0.4 m compared to the signal in water and seems to consist of two peaks. This could indicate a contribution from the moving surface caused by the oscillating air bubble (scenario 2) as the time delay of the motion of the water surface is expected to increase more with increasing source depths compared to the sound transmission. This could be explained by the lower wall velocity of the expanding bubble of ≤ 100 m/s, estimated from modeling, compared to the sound velocity in water of 1500 m/s. However, as the camera recordings are not synchronized with the trigger system of the seismic source it is difficult to quantify this effect.

For a comparison of both experiments we estimate the acoustic signal that is transmitted into air depending on the source-interface distance as the ratio between the maximum amplitude in air and water (Fig. 6). The error bars indicate the computed standard deviation of the ratio from the measured data. The theoretical amplitude ratio using the plane wave transmission coefficient T_p for vertical incidence on the water surface is shown as a reference. The data seem to converge toward the plane wave transmission coefficient with increasing ratios of z_s/R_m which means that the source is at a large depth or the bubble radius of the source is small.

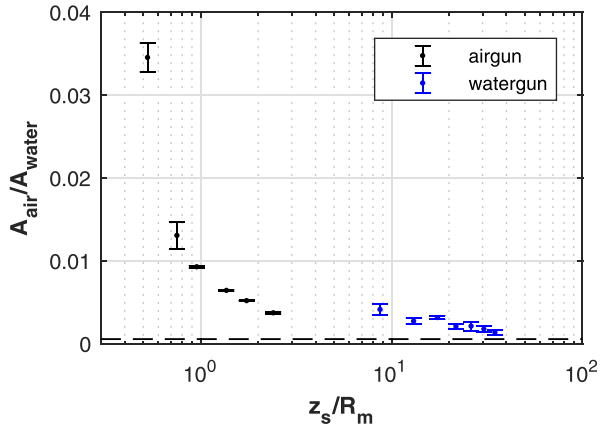

FIG. 6. (Color online) Ratio of maximum peak amplitude measured in air A_{air} and water A_{water} for both experiments depending on the ratio between the source depth z_s and maximum bubble size R_m. R_m is replaced with R_{mc} and R_{mb} for the respective experiment. Computed for a 300 Hz low-pass filtered signal. Dashed line shows theoretical ratio using the plane wave transmission coefficient T_p.

The amplitude ratio strongly increases when $z_s/R_m < 1$. It should be noted that the source bubble interacts with the interface for small z_s/R_m values and hence the plane wave transmission coefficient might not be a fair comparison. However, it acts as a descriptive reference. It should be noted that the stronger amplitude ratios of the airgun experiment can be due to two mechanisms. First, an increased transmission caused by the smaller ratio of z_s/R_m as theoretically demonstrated by Godin (2008). Second, due to the interaction of the bubble with the water surface which also can emit sound waves into the air (scenarios 2 and 3)? In contrast, there is no direct interaction between the source and water–air interface in the watergun experiment (scenario 1).

Two further observations from experiment B are discussed in the following. First, an interaction between the source and the water–air interface is expected for all depths as the deepest source depth of 0.6 m is less than 2.5 times the maximum bubble radius R_{mb} and hence it is within the critical range for interaction (Chahine, 1977). The impact of the airgun bubble on the water–air interface can be observed in Fig. 7(a). The photos show the surface lift due to the expanding airgun bubble (scenario 2). The variation of the maximum surface lift with time is measured from the videos and marks on the rope [Fig. 7(b)]. Each still photo of the video, every 4.2 ms, was inspected and the maximum lift, max(h), was measured from the ruler indicated in Fig. 7(a). Only two videos for each source depth are evaluated and the estimation of the shallowest sources, $z_s < 0.3$ m, is more a guess due to the splash and other non-linear effects. However, we get a rough estimate for the surface elevation and the estimation for the deeper sources could be performed more accurately for the first bubble oscillation. We note how the surface lift decreases with increasing source depth. In addition, the correlation of the maximum bubble radius and maximum surface displacement can be observed. The maximum bubble radius is reached when the acoustic pressure has a minimum [Fig. 7(b), gray line]. We also note that the surface is almost instantly lifted when the gun is fired. It should be noted that the gun trigger and video recording are not synchronized. We estimate time zero for the video recordings from the first sign of released air from the gun.

Second, we investigate the measured signal in air at different angles between the vertical line through the source and the plane from the water–air interface to the receiver. Therefore, we compare the recorded signals measured at H_2, H_3, and H_4 (Fig. 3) within different frequency filter bands (Fig. 8). We observe that the signals are almost the same at all receivers for the lowest frequency band, below 50 Hz, while the difference increases with increasing frequency. When comparing the amplitudes, we observe that receiver H_4 records stronger signals at higher frequencies compared to the other two receivers. The shape of the recorded signal is similar at all receivers and in all frequency bands within the first 0.3 s. At later times the differences between the recordings increase, especially between

https://doi.org/10.1121/10.0000691

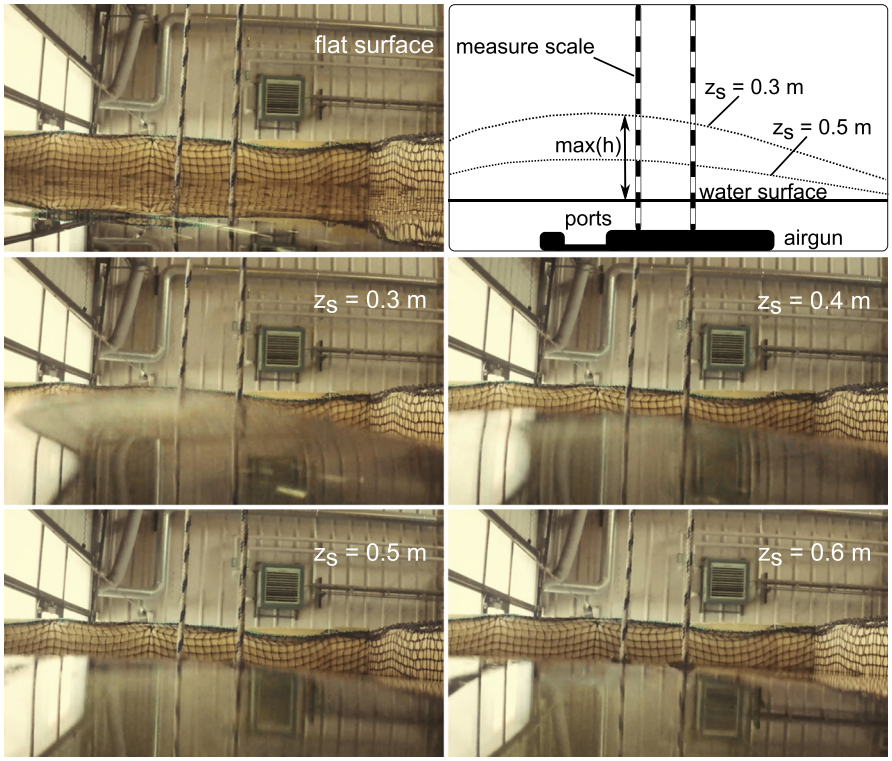

(a)

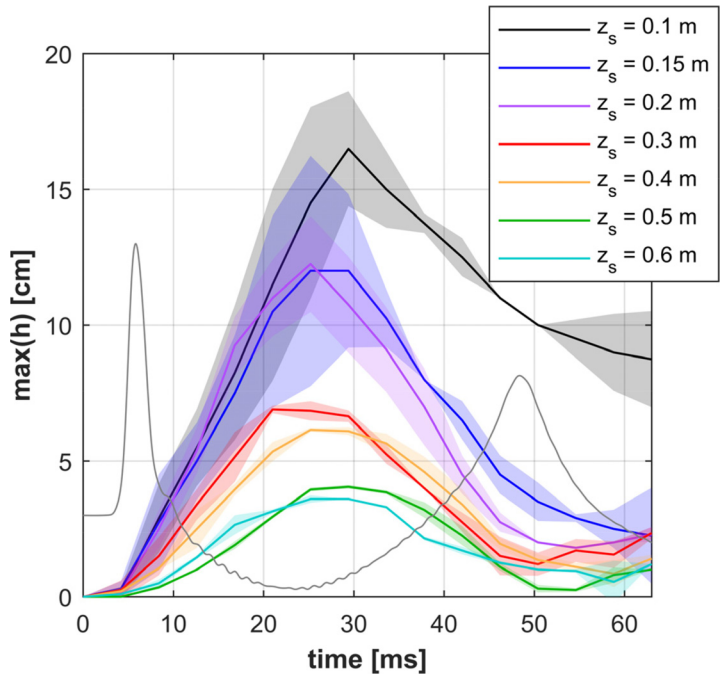

(b)

FIG. 7. (Color online) (a) Photos at water surface for airgun experiment B fired at different source depths z_s taken ca. 20 ms after air gun is triggered, when bubble radius R is close to its maximum. Sketch shows the setup and how max(h) is measured. (b) Measured maximum surface displacement h for different source depths. Shaded area indicates the error. Gray line is the normalized measured acoustic pressure in water for the airgun fired at $z_s = 0.3$ m.

receiver H_4 and the other two hydrophones (H_2, H_3). These variations could be explained by reflections from different obstacles in air inside the work hall as the receivers are located at different positions. While reflections might also impact the amplitudes, further explanations for these differences are evaluated in Sec. V. The results are compared to the findings of Godin (2008) and Calvo *et al.* (2013) which demonstrate that the transmission into air depends on the source-interface distance and the wavelength of the signal.

B. Comparing modeled and measured signatures

We compare the measured data to a simple model to explain the acoustic signal in air observed in experiment B (Fig. 5). The signal might be partially explained by the

movement of the water surface and the bubble venting into the surrounding air when it breaks the surface, in addition to the acoustic signal that is directly transmitted through the water–air interface. The effect is investigated using the phenomenological model that describes the movement of the water surface as a function of the bubble radius [Eq. (3)]. We compute the airgun bubble parameter in water using a damped Kirkwood-Bethe equation as (Kirkwood and Bethe, 1942; Landrø and Sollie, 1992; Ziolkowski, 1970)

$$\ddot{R}=\frac{\left(1+\frac{\dot{R}}{C}\right)H+\left(1-\frac{\dot{R}}{C}\right)\frac{R}{C}\dot{H}-\frac{3}{2}\left(1-\frac{\dot{R}}{3C}\right)\dot{R}^2-\alpha\dot{R}+\beta\dot{R}^2}{R\left(1-\frac{\dot{R}}{C}\right)}, \tag{5}$$

where R, $\dot{R}$, and $\ddot{R}$ are the bubble radius, velocity, and acceleration, respectively. The sound velocity in water at the bubble wall is denoted by C, H is the enthalpy, and α and β are damping and empirical coefficients accounting for energy losses of the bubble oscillation. We adjust the damping parameters to fit the measurements in water at H_1 (Fig. 3). In addition, we assume that the bubble breaks the surface and vents into the air when a critical bubble radius R_c is reached depending on the source depth. This radius is assumed to be $R_c = 1.5z_s$ estimated from the video observations and acoustic recordings in water. We assume that the growth of the bubble radius and hence the surface displacement stops abruptly when the critical radius is reached (Fig. 9). Although this is a very simplistic model, we observe on the video recordings that the bulge at the water surface for the shallowest source depth of $z_s = 0.1$ m is kept almost constant for a long time compared to the deeper sources (Figs. 13 and 14). Similar observations for an almost stationary water surface displacement during a collapsing cavity are demonstrated by Robinson *et al.* (2001).

The surface displacement h is computed using Eq. (3) and the general shape of the water surface is explained well by this *ad hoc* model. We note that the similarity between the modelled and measured surface displacement is also due to the fact that we have adjusted Eq. (3) to our experiments as mentioned in Sec. II. The acoustic signal at the receiver can be computed from the surface movement using Eq. (2). The model and measurements are compared in Fig. 10. A lower high-cut filter than in Fig. 5 is used as higher frequencies are more complicated to model due to the splash and other non-linear effects at the water surface. Differences between the measurements and model could be due to the assumption of an abrupt stop of the bubble radius which is way more complex in practice compared to the simple model used to describe the surface lift. This point needs to be investigated in more detail to quantify the amplitudes as the breaking point is crucial for that purpose. However, the general shape with the negative peak in air could be reproduced by the model (Fig. 10). The negative peaks in air for the depths of 0.1 and 0.15 m are explained by the negative acceleration of the surface displacement caused by the abrupt stop of the bubble (Fig. 9) (scenario 3). When the bubble does not break the surface immediately, at 0.3 m, the signal in air is a repetition of the bubble movement in water (scenario 2). Hence, the movement of the water surface

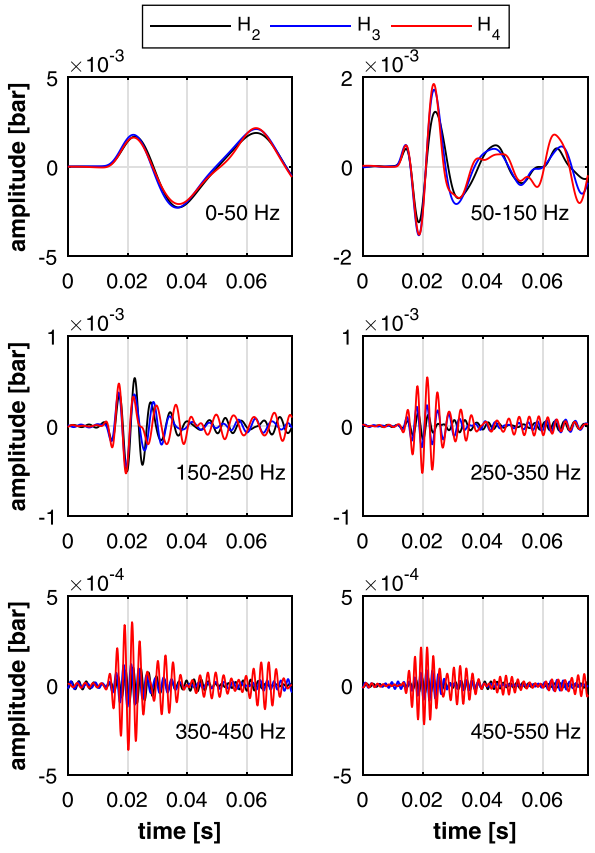

FIG. 8. (Color online) Measurements of airgun signature in air at H_2, H_3, and H_4 (Fig. 3) with different bandpass filters applied as indicated, corrected for spreading with $1/r$ and aligned in time. The source depth is $z_s = 0.3$ m. Note the different amplitude scales for the each plot.

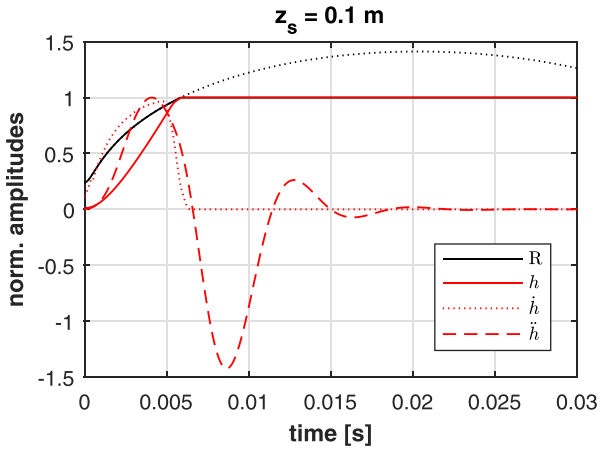

FIG. 9. (Color online) Modelled bubble radius R and surface displacement h vertically above the source. The critical radius R_c, when the bubble breaks the surface, is reached at 1. The black dotted line indicates the modelled bubble radius if it had not broken the water–air interface. A 150 Hz low-pass filter is applied to $\ddot{h}$. Each value is normalized to its own maximum value, respectively.

https://doi.org/10.1121/10.0000691

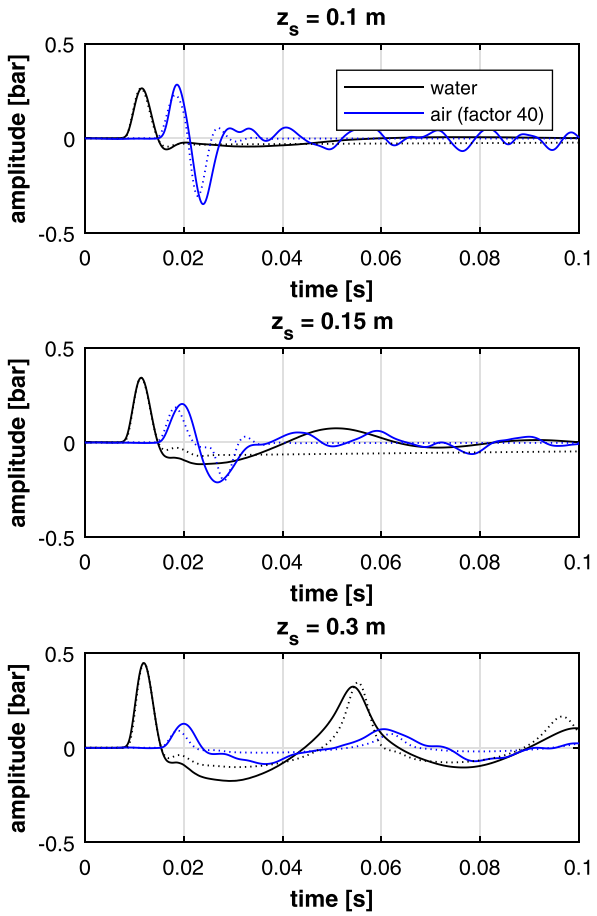

FIG. 10. (Color online) Measured (solid) and modelled (dotted) signals from the 12 in^3 airgun recorded in water at H_1 and in air at H_4 as indicated in Fig. 3 for different source depths z_s. A 150 Hz low-pass filter is applied to the data.

contributes to the signal in air for very shallow source depths. Similar signals and mechanisms are discussed by Bowman *et al.* (2014) who conduct experiments with small explosives at different burial depths close to the surface. Although they investigate the coupling between an elastic medium and air, some phenomena seem to be similar. Furthermore, investigations on volcanic eruptions conducted in the field of infrasound reveal similar acoustic signals received in air (Johnson, 2003; Yokoo and Iguchi, 2010).

V. DISCUSSION

First, we discuss potential mechanisms that could explain the amplitude differences observed in Fig. 8. Second, we elaborate more on the observations of the water–air interface while the airgun in experiment B is fired.

One explanation for the higher amplitudes with higher frequencies measured at receiver H_4 compared to the receivers H_2 and H_3 (Fig. 8) might be evanescent waves in water which are transmitted as homogeneous waves into air. As discussed for a monopole sound source by Godin (2008) and Calvo *et al.* (2013) more signal could be transmitted into air with decreasing frequencies and source depths when $z_s/\lambda \ll 1$, where λ is the wave length in water. Calvo *et al.* (2013) compute the transmitted signal into air using wave-number integration which demonstrates that most of the signal is confined inside a cone, when only homogeneous waves in water are assumed (Fig. 11). The angle of the cone corresponds to the critical angle between water and air. When evanescent waves are taken into account, the radiation into air is close to omnidirectional for small z_s/λ ratios as shown for an example with the ratio $z_s/\lambda = 0.034$ by Calvo *et al.* (2013). In our experiments (Fig. 8) the ratio is $z_s/\lambda = 0.005$ for the lowest frequency band, assuming

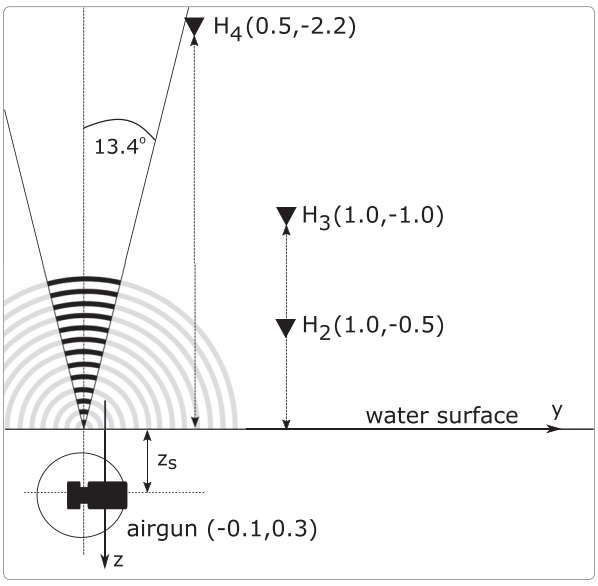

FIG. 11. Two-dimensional (2D) section of experimental setup shown in Fig. 3. The transmitted signal into air from a monopole sound source is sketched accounting only for homogeneous waves (black line) and including the evanescent part (gray line), adopted from Calvo *et al.* (2013).

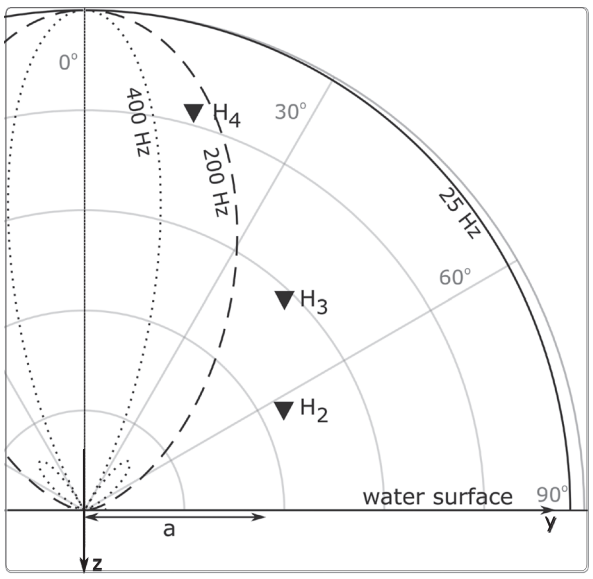

FIG. 12. 2D section of experimental setup shown in Fig. 3. The directivity for a vibrating baffled piston is shown schematically for three different frequencies. The piston radius is denoted as a and arbitrary amplitudes are assumed.

$f = 25$ Hz, while it is $z_s/\lambda = 0.1$ for the highest frequency range, assuming $f = 500$ Hz. Therefore, evanescent waves might be one explanation that we observe the same signal amplitude at all receivers for the lowest frequencies. For the highest frequencies, when the evanescent component is less pronounced, the amplitudes are stronger close to the 13.4° cone, which is the case for receiver H_4 (Fig. 8). It should be noted that the theory is developed for a monopole sound source which is not fully valid for the airgun fired close to the interface.

Another explanation for the higher amplitudes with higher frequencies measured at receiver H_4 compared to receivers H_2 and H_3 (Fig. 8) could be the radiation pattern of the moving water surface. If we assume that the water surface acts like a loudspeaker or a circular baffled piston, the directivity of the emitted sound depends on the frequency (Hambric and Fahnline, 2007; Morse and Ingard, 1986). The variations of the radiated acoustic signal with frequency are schematically shown in Fig. 12. For simplicity, we estimate the far-field acoustic pressure from a baffled piston as (Hambric and Fahnline, 2007)

$$p_i(r_i, \theta_i) = i\omega\rho_a a^2 v \left[\frac{J_1(k_a a \sin(\theta_i))}{k_a a \sin(\theta_i)}\right] \frac{e^{-ikr_i}}{r_i}, \quad (6)$$

where v is the piston velocity and a its radius, and J_1 is the first order Bessel function. The angle and distance between the origin of the coordinate system and specific hydrophone $i = 2, 3, 4$ is denoted as θ_i and r_i, respectively (Fig. 12). It should be noted that the moving water surface in the experiment is varying in size while a constant piston size is assumed in the model. We compute the theoretical amplitude ratios p_4/p_3 and p_4/p_2 for three different frequencies to estimate the relative variations of the amplitude between the hydrophones. For 50 Hz the ratios are $p_4/p_3 \approx p_4/p_2 \approx 1$, for 200 Hz the ratios are $p_4/p_3 \approx 3$ and $p_4/p_2 \approx 10$, and for 400 Hz the ratios are $p_4/p_3 \approx 5$ and $p_4/p_2 \approx 83$. If we compare the ratios with the measured results in Fig. 8, we note that they agree well for the lowest frequency of 50 Hz. For higher frequencies the ratios for p_4/p_3 of 3 and 5 are still comparable with the measured amplitudes while the computed ratios for p_4/p_2 does not agree with the observed results. Therefore, this effect could partially explain the

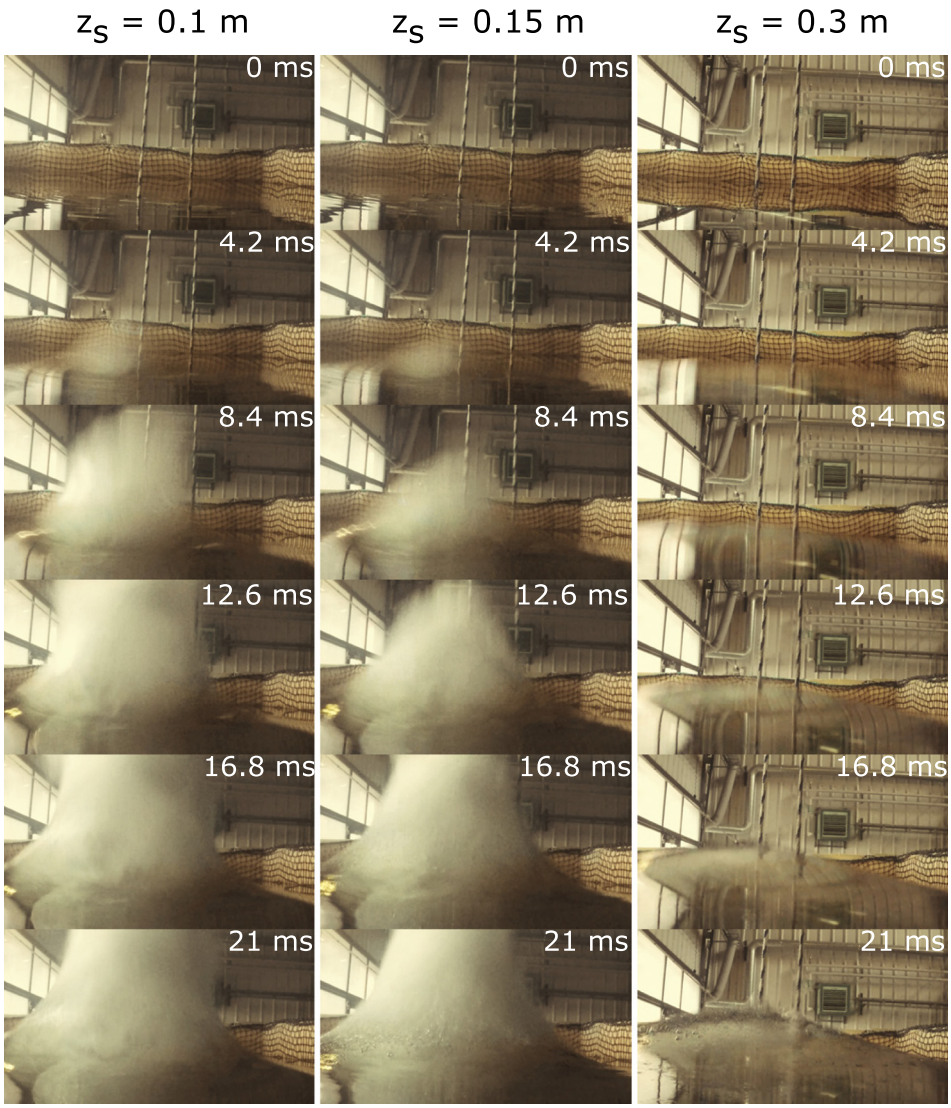

FIG. 13. (Color online) Photos of airgun fired at a different source depths z_s taken at different times as indicated. The source depths correspond to the recordings shown in Fig. 10. Pressure recordings and camera are not synchronized.

https://doi.org/10.1121/10.0000691

observations while the mechanisms become more complex with increasing frequencies.

For a more detailed investigation of the impact on the water–air interface in experiment B photos from the video recordings are shown for three different source depths (Figs. 13 and 14). In these figures we note that the water surface has already changed for all source depths for time instants between 0 and 4.2 ms. A white foam lifted from the surface is visible at 4.2 ms for source depths of 0.1 and 0.15 m that is not visible for the 0.3 m source depth. That might be water vapor molecules lifted from the surface due to the high pressure incident on the water–air interface (Loveridge, 1985). In addition, we note that water droplets are created above the water surface starting at approximately 21 ms. This observation can be best recognized when the photos at 21 ms (Fig. 13) and 25.2 ms (Fig. 14) for a source depth of 0.3 m are compared. The time correlates with the beginning contraction of the airgun bubble and hence the downward movement of the water–air interface [Fig. 7(b)]. The large surface spike at the center above the bubble, generated for source depths of 0.1 and 0.15 m over time (Figs. 13 and 14), is also demonstrated by many authors for the interaction of spark- or laser-induced cavities with the water–air interface (Blake and Gibson, 1981; Longuet-Higgins, 1983; Robinson *et al.*, 2001) and for underwater explosions (Rogers and Szymczak, 1997). An experimental study of underwater detonations close the water surface is conducted by Craig (1974). The strong surface lift is associated with a jet formation that is directed away from the free surface and propagates through the center of the bubble (Gibson, 1968; Robinson *et al.*, 2001; Supponen *et al.*, 2015; Zhang and Liu, 2015). The surface spike and jet are caused by a high pressure region between the bubble and free surface (Pearson *et al.*, 2004) and hence the pressure above the bubble is larger than below. If we assume that the bubble directly bursts at the water–air interface, one might expect that the jet is directed toward the surface again. The evolution and height of the surface spike for collapsing cavities is investigated by Longuet-Higgins (1983) and Pearson *et al.* (2004). It should be noted that there are two main differences between cavities or underwater explosions and the bubble generated by an airgun. These are the existence of

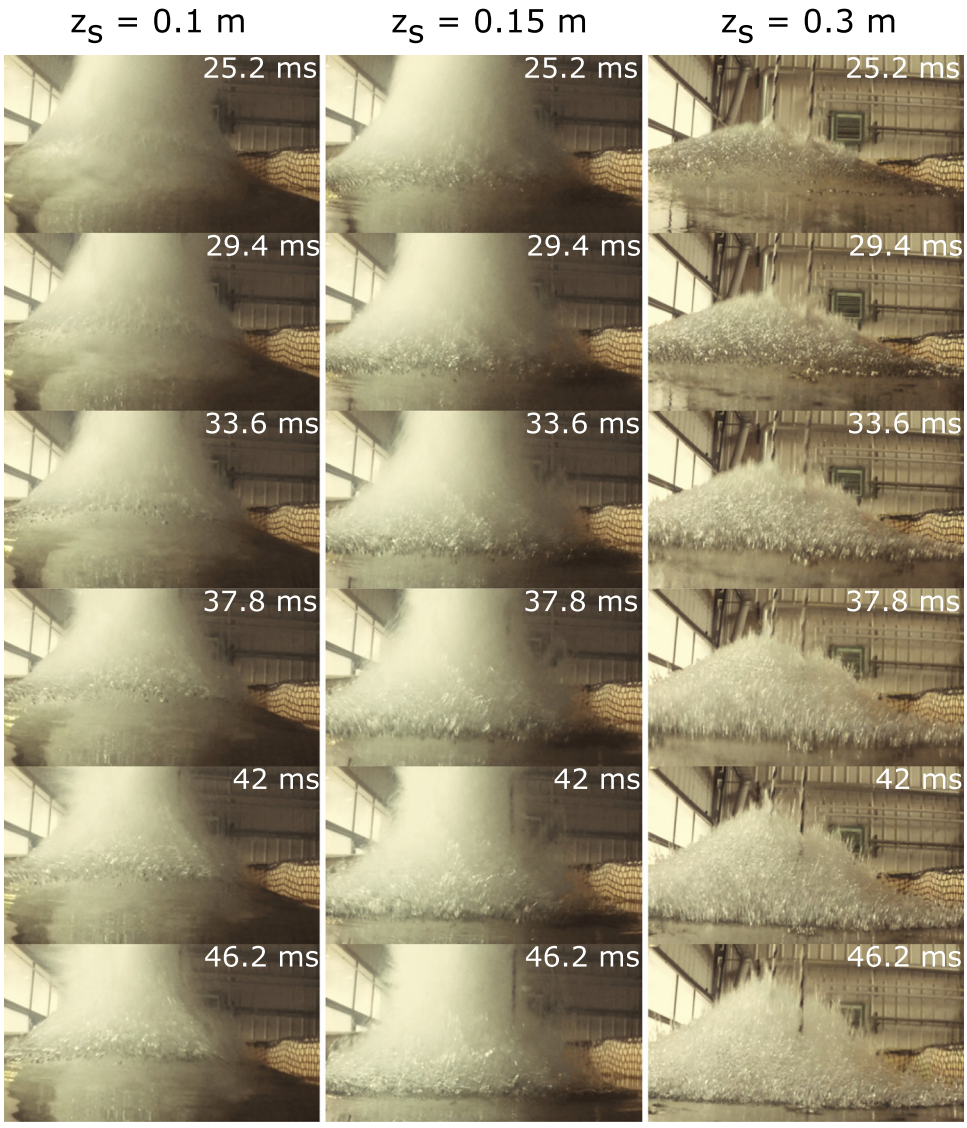

FIG. 14. (Color online) Continuation of Fig. 13.

the airgun body at the bubble center and the shape of the bubble that is not exactly spherical due to the gun ports of an airgun (de Graaf *et al*., 2014; Langhammer and Landrø, 1996). How this could impact the bubble oscillation in the vicinity of a free surface is experimentally investigated for a laboratory scale airgun by de Graaf *et al*. (2014).

VI. CONCLUSION

Our experiments show that the interaction of very shallow marine seismic sources with the water–air interface contributes significantly to the acoustic signal emitted into air. The model and measurements indicate that the moving water surface, caused by the interaction of the water surface with the oscillating bubble, and the breaking of the bubble at the water surface contribute to the signal in air similar as from a vibrating membrane. In addition, we observe that the radiation pattern of the acoustic signal in air gets closer to omnidirectional for decreasing source depths and frequencies. The acoustic signal in air from a small cavity is about 300–600 times weaker than the signal in water for frequencies lower than 300 Hz. This is valid for a cavity that is sufficiently far away from the water–air interface so that there is no interaction between the cavity and the water surface. For a bigger airgun bubble the acoustic signal in air is about 40–300 times weaker than the signal in water for frequencies lower than 300 Hz. The stronger acoustic signal in air is caused by the emitted sound pressure waves from the moving water surface, in addition to the directly transmitted acoustic signal. For very shallow airgun depths the signal consists of a positive peak followed by a negative peak of the same magnitude. The negative peak is attributed to the breaking of the water–air interface as demonstrated in the modeling, and supported by high speed photos. To quantify the contributions from the moving surface to the acoustic signal measured in air, the mechanism needs to be investigated in more detail. However, the experimental results are helpful to understand the behaviour of seismic sources fired close to the surface and how the acoustic signal in air is generated. These findings could lead to new considerations in the setup of marine seismic sources and might improve seismic processing as the source signal is better understood.

ACKNOWLEDGMENTS

We acknowledge the European Union's Horizon 2020 research and innovation programme under the Marie Skłodowska-Curie Grant Agreement No. 641943 for the funding of D.W.'s Ph.D. project within WAVES. We would like to acknowledge the technical team at IGP for their support to the experimental setup. M.L. thanks the Norwegian Research Council and the industry partners of the GAMES consortium at NTNU for financial support (Grant No. 294404). We would also like to acknowledge the helpful comments from two unknown reviewers that have improved the manuscript at several points.

Aki, K., and Richards, P. G. (**2002**). *Quantitative Seismology* (University Science Books, Mill Valley, CA).
Amundsen, L., Westerdahl, H., Pedersen, Å. S., Thompson, M., and Landrø, M. (**2017**). "On firing an air gun very shallow," Geophys. **82**(3), A25–A29.
Ballhaus, W. F., Jr., and Holt, M. (**1974**). "Interaction between the ocean surface and underwater spherical blast wave," Phys. Fluids **17**(6), 1068–1079.
Blake, J. R., and Gibson, D. C. (**1981**). "Growth and collapse of a vapour cavity near a free surface," J. Fluid Mech. **111**, 123–140.
Boulton-Stone, J. M., and Blake, J. R. (**1993**). "Gas bubbles bursting at a free surface," J. Fluid Mech. **254**, 437–466.
Bowman, D. C., Taddeucci, J., Kim, K., Anderson, J. F., Lees, J. M., Graettinger, A. H., Sonder, I., and Valentine, G. A. (**2014**). "The acoustic signatures of ground acceleration, gas expansion, and spall fallback in experimental volcanic explosions," Geophys. Res. Lett. **41**(6), 1916–1922, https://doi.org/10.1002/2014GL059324.
Brekhovskikh, L. M., and Lysanov, Y. P. (**1991**). *Fundamentals of Ocean Acoustics* (Springer, New York).
Calvo, D. C., Nicholas, M., and Orris, G. J. (**2013**). "Experimental verification of enhanced sound transmission from water to air at low frequencies," J. Acoust. Soc. Am. **134**(5), 3403–3408.
Chahine, G. L. (**1977**). "Interaction between an oscillating bubble and a free surface," J. Fluids Eng. **99**(4), 709–716.
Chahine, G. L., Frederick, G. S., Lambrecht, C. J., Harris, G. S., and Mair, H. U. (**1995**). "Spark generated bubbles as laboratory-scale models of underwater explosions and their use for validation of simulation tools," in *Proceedings of the 66th Shock and Vibration Symposium*, Biloxi, MS, Vol. 2, pp. 265–276.
Chan, B. C., Holt, M., and Welsh, R. L. (**1968**). "Explosions due to pressurized spheres at the ocean surface," Phys. Fluids **11**(4), 714–722.
Cinbis, C., Mansour, N. N., and Khuri-Yakub, B. T. (**1993**). "Effect of surface tension on the acoustic radiation pressure-induced motion of the water-air interface," J. Acoust. Soc. Am. **94**(4), 2365–2372.
Collins, R., and Holt, M. (**1968**). "Intense explosions at the ocean surface," Phys. Fluids **11**(4), 701–713.
Craig, B. G. (**1974**). "Experimental observations of underwater detonations near the water surface," University of Carolina, Report LA-5548-MS.
Cui, P., Zhang, A. M., and Wang, S. P. (**2016**). "Small-charge underwater explosion bubble experiments under various boundary conditions," Phys. Fluids **28**(117103), 1–24.
de Graaf, K. L., Brandner, P. A., and Penesis, I. (**2014**). "The pressure field generated by a seismic airgun," Exp. Therm. Fluid Sci. **55**, 239–249.
Gibson, D. C. (**1968**). "Cavitation adjacent to plane boundaries," in *Proceedings of the 3rd Australian Conference on Hydraulics and Fluid Mechanics*, Sydney, Australia, pp. 210–214.
Glushkov, E. V., Glushkov, N. V., and Godin, O. A. (**2013**). "The effect of anomalous transparency of the water-air interface for a volumetric sound source," Acoust. Phys. **59**(1), 6–15.
Godin, O. A. (**2006**). "Anomalous transparency of water-air interface for low-frequency sound," Phys. Rev. Lett. **97**(16), 164301.
Godin, O. A. (**2008**). "Sound transmission through water-air interfaces: New insights into an old problem," Contemp. Phys. **49**(2), 105–123.
Hambric, S. A., and Fahnline, J. B. (**2007**). "Structural acoustics tutorial-part 2: Sound-structure interaction," Acoust. Today **3**(2), 9–27.
Harris, G. R. (**1981**). "Transient field of a baffled planar piston having an arbitrary vibration amplitude distribution," J. Acoust. Soc. Am. **70**(1), 186–204.
Hung, C. F., and Hwangfu, J. J. (**2010**). "Experimental study of the behaviour of mini-charge underwater explosion bubbles near different boundaries," J. Fluid Mech. **651**, 55–80.
Johnson, J. B. (**2003**). "Generation and propagation of infrasonic airwaves from volcanic explosions," J. Volcanol. Geoth. Res. **121**(1–2), 1–14.
Kinsler, L. E., Frey, A. R., Coppens, A. B., and Sanders, J. V. (**1962**). *Fundamentals of Acoustics*, 4th ed. (John Wiley & Sons, Inc., New York).
Kirkwood, J. G., and Bethe, H. A. (**1942**). "Shock and detonation waves," U.S. Office of Scientific Research and Development (OSRD), Report 588.
Krieger, J. R., and Chahine, G. L. (**2005**). "Acoustic signals of underwater explosions near surfaces," J. Acoust. Soc. Am. **118**(5), 2961–2974.
Landrø, M., and Amundsen, L. (**2014**). "Is it optimal to tow air guns shallow to enhance low frequencies?," Geophys. **79**(3), A13–A18.

Landrø, M., and Sollie, R. (**1992**). "Source signature determination by inversion," Geophys. **57**(12), 1633–1640.
Langhammer, J., and Landrø, M. (**1996**). "High-speed photography of the bubble generated by an airgun," Geophys. Prospect. **44**, 153–173.
Li, J., Wang, S., Tao, Y., Dong, C., and Tang, G. (**2017a**). "A novel expression of the spherical-wave reflection coefficient at a plane interface," Geophys. J. Int. **211**, 700–717.
Li, J., Wang, S., Wang, J., Dong, C., and Yuan, S. (**2017b**). "Frequency-dependent spherical-wave reflection in acoustic media: Analysis and inversion," Pure Appl. Geophys. **174**, 1759–1778.
Longuet-Higgins, M. S. (**1983**). "Bubble, breaking waves and hyperbolic jets at the free surface," J. Fluid Mech. **127**, 103–121.
Loveridge, M. M. (**1985**). "Marine seismic source signatures, directivity and the ghost," Ph.D. thesis, University of Oxford.
Lu, N. Q., Oguz, H. N., and Prosperetti, A. (**1989**). "The oscillations of a small floating bubble," Phys. Fluids A **1**, 252–260.
Lubard, S. C., and Hurdle, P. M. (**1976**). "Experimental investigation of acoustic transmission from air into a rough ocean," J. Acoust. Soc. Am. **60**(5), 1048–1052.
McDonald, B. E., and Calvo, D. C. (**2007**). "Enhanced sound transmission from water to air at low frequencies (L)," J. Acoust. Soc. Am. **122**(6), 3159–3161.
Morse, P. M., and Ingard, K. U. (**1986**). *Theoretical Acoustics* (McGraw-Hill Book Company, New York).
Oguz, H. N., and Prosperetti, A. (**1990**). "Bubble oscillations in the vicinity of a nearly plane free surface," J. Acoust. Soc. Am. **87**(5), 2085–2092.
Pearson, A., Cox, E., Blake, J. R., and Otto, S. R. (**2004**). "Bubble interactions near a free surface," Eng. Anal. Bound. Elem. **28**, 295–313.
Rayleigh, O. M. (**1917**). "On the pressure developed in a liquid during the collapse of spherical cavity," Philos. Mag. Ser. **34**(200), 94–98.
Robinson, P. B., Blake, J. R., Kodama, T., Shima, A., and Tomita, Y. (**2001**). "Interaction of cavitation bubbles with a free surface," J. Appl. Phys. **89**(12), 8225–8237.
Rogers, J. C. W., and Szymczak, W. G. (**1997**). "Computations of violent surface motions: Comparisons with theory and experiment," Philos. Trans. Royal Soc. London A **355**(1724), 649–663.
Sohn, R. A., Vernon, R., Hildebrandt, J. A., and Webb, S. C. (**2000**). "Experimental investigation of acoustic transmission from air into a rough ocean," J. Acoust. Soc. Am. **107**(6), 3073–3083.
Supponen, O., Kobel, P., Obreschkow, D., and Farhat, M. (**2015**). "The inner world of a collapsing bubble," Phys. Fluids **27**, 091113.
Vergniolle, S., and Brandeis, G. (**1994**). "Origin of the sound generated by Strombolian explosions," Geophys. Res. Lett. **21**(18), 1959–1962, https://doi.org/10.1029/94GL01286.
Vergniolle, S., and Brandeis, G. (**1996**). "Strombolian explosions 1. A large bubble breaking at the surface of a lava column as a source of sound," J. Geophys. Res. **101**(B9), 20433–20447, https://doi.org/10.1029/96JB01178.
Vergniolle, S., Brandeis, G., and Mareschal, J.-C. (**1996**). "Strombolian explosions 2. Eruption dynamics determined from acoustic measurements," J. Geophys. Res. **101**(B9), 20449–20466, https://doi.org/10.1029/96JB01925.
Voloshchenko, A. P., and Tarasov, S. P. (**2013**). "Effect of anomalous transparency of a liquid-gas interface for sound waves," Acoust. Phys. **59**(2), 163–169.
Voloshchenko, A. P., and Tarasov, S. P. (**2019**). "Experimental study of the transmission of low-frequency acoustic waves through a water-air interface," J. Acoust. Soc. Am. **145**(143), 143–148.
Wang, S. P., Zhang, A. M., Liu, Y. L., Zhang, S., and Cui, P. (**2018**). "Bubble dynamics and its applications," J. Hydrodyn. **30**(6), 975–991.
Wehner, D., Landrø, M., and Amundsen, L. (**2019**). "On low frequencies emitted by air guns at very shallow depths—An experimental study," Geophys. **84**(5), P61–P71.
Wehner, D., Landrø, M., Amundsen, L., and Westerdahl, H. (**2018**). "Frequency-depth-dependent spherical reflection response from the sea surface—a transmission experiment," Geophys. J. Int. **214**, 1206–1217.
Yan, B. P., Wang, S. X., Yuan, S. Y., Ji, Y. Z., and Tao, Y. H. (**2017**). "Frequency-dependent reflection coefficient of spherical wave in acoustic medium," in *79th EAGE Conference & Exhibition*, Tu P1 10.
Yokoo, A., and Iguchi, M. (**2010**). "Using infrasound waves from eruption video to explain ground deformation preceding the eruption of Suwanosejima volcano, Japan," J. Volcanol. Geoth. Res. **196**(3–4), 287–294.
Zhang, A. M., and Liu, Y. L. (**2015**). "Improved three-dimensional bubble dynamics model based on boundary element method," J. Comput. Phys. **294**, 208–223.
Ziolkowski, A. (**1970**). "A method for calculating the output pressure waveform from an air gun," Geophys. J. Royal Astronom. Soc. **21**, 137–161.